COBEM 2021 26th International Congress of Mechanical Engineering
November 22-26, 2021, Virtual Congress, Brazil
ABCM Associação Brasileira de Engenharia e Ciências Mecânicas

COB-2021-0179
MODEL BASED AIRFLOW ANGLE ESTIMATION USING GPS/INS SENSOR FUSION AND APPLICATION TO UNMANNED AIRCRAFT VEHICLE

M.Eng. Lucas Moraes Santos
Instituto Tecnológico de Aeronáutica
lucasmoraes90@hotmail.com

Dr. Luiz Carlos Sandoval Góes
Instituto Tecnológico de Aeronáutica
goes@ita.br

M.Sc. Juliano Augusto de Bonfim Gripp
Embraer
juliano.gripp@embraer.com

Abstract. *This work presents two methods for estimating the True Airspeed, Angle of Attack, and Sideslip Angle of a fixed-wing aircraft, using data from inertial sensors. The first estimation method was based on approximations of the aircraft's vertical and lateral accelerations to synthesize Angle of Attack and Sideslip Angle data. The estimation of the True Airspeed for this method was made based on the approximation of the inertial speed. The second estimation method was based on the Extended Kalman Filter, a near-optimal state estimator for non-linear systems. With this Filter, aside from the True Airspeed, Angle of Attack, and Sideslip Angle, it was possible to estimate the Wind Speed and Direction. The estimation techniques were tested using synthetic flight data produced from flight simulations, and using flight test data. Simulations ran in MATLAB®, solving the dynamic equations and employing the aerodynamic model for the C2 Unmanned Aerial Vehicle. The flight test data was also from the C2 UAV. The estimation results for the two methods are presented, compared, and discussed.*

Keywords: *Synthetic air data, Airflow angle estimation, Unmanned air vehicle.*

1. INTRODUCTION

Air data consists of all the aerodynamic variables that are necessary for the correct guidance, navigation, and control of aircraft. They may consist of Mach number, pressure altitude, true air temperature, true airspeed, angle of attack, sideslip angle, and others Edward A. Haering (1995).

True airspeed (represented as V) is the speed of the aircraft in relation to the atmosphere. In a still atmosphere, which does not move in relation to the ground, the true airspeed will be the same as the speed of the aircraft in respect to the ground, also known as the ground speed. In a moving atmosphere, which means the wind is present, the true airspeed is the difference between the aircraft's ground speed and the wind speed.

The angle of attack measurement (AoA, represented by the Greek letter α) is the angle between the airspeed projection in the aircraft plane of symmetry (xz-plane) and its longitudinal axis (or x-axis), and it is of utmost importance for the safety of flight. High angles of attack may lead to the separation of the airflow around the wing, causing a great reduction in the lift coefficient and, therefore, the lift force. This is also known as stall. Given a certain speed greater than the stall speed, the lift coefficient can be increased by increasing the aircraft angle of attack up to the critical AoA, when a stall happens. The stall will cause the aircraft to lose altitude rapidly, and, if the lift is not recovered in time, it may lead to a catastrophic event.

The sideslip angle (SSA, represented by the Greek letter β) is responsible for the lateral forces that may lead to oscillations, like the Dutch roll. From the perspective of aircraft dynamics, these oscillations are typically stable. This means they will diminish over time and will not lead to an overall unstable flight, but they are uncomfortable to passengers and will cause unnecessary structural stress to the airframe. It is measured as the angle between the airspeed and the aircraft xz plane.

For small Unmanned Aerial Vehicles (UAV), the total removal of anemometric sensors is desirable due to the difficulties of installing these sensors in a reduced airframe. The fragility of the airframe and its small dimensions pose a

challenge to align the probes with the airflow, which may compromise accuracy. Also, anemometric sensors must be calibrated to offset the effects of the aircraft-induced airflow around itself Moes and Whitmore (1990). An extensive calibration campaign is necessary to minimize the errors of Pitot pressures, static pressures, temperature, flow angle, AoA, and sideslip angle measurements Edward A. Haering (1995). This campaign starts with wind tunnel experiments but may be extended to in-flight measurements and may include tower fly-bys, the use of trailing cone, pacer aircraft, radar tracking, among others. To achieve a desirable level of accuracy, high investment is necessary and may hinder a small UAV project.

In respect to its operation, small UAVs and other aircraft with higher maneuverability, such as jet fighters and aerobatic aircraft, experience high angle-of-attack during certain maneuvers. Calibration of anemometric sensors is usually done for steady-state effects, which causes large errors due to unmodeled aerodynamic effects Moes and Whitmore (1990). Also, the low-frequency response associated with the unsteady conditions of high angle of attack flight may lead to inaccurate air data.

In this work, two model-based methods for estimating airflow angles will be presented. These methods will use data from the Global Positioning System unit and Inertial Navigation System sensors to estimate the angles and airspeed of an unmanned aircraft vehicle in the early stages of its aircraft model identification campaign. The methods will be compared, and their limitations of use will be addressed.

2. MATHEMATICAL MODEL

2.1 Translation dynamics

The translational equations which define the model can be obtained through Newton's Second Law for linear motion. In the Body Reference Frame (BRF), the equations can be rearranged to express the body accelerations in the longitudinal axis ($\dot{u}$, Equation 1), lateral axis ($\dot{v}$, Equation 2), and vertical axis ($\dot{w}$, Equation 3).

$$\dot{u} = r\,v - q\,w + F_x \tag{1}$$
$$\dot{v} = p\,w - r\,u + F_y \tag{2}$$
$$\dot{w} = q\,u - p\,v + F_y \tag{3}$$

Where u, v, and w are the longitudinal, lateral, and vertical speeds in the BRF respectively; p, q, and r are the roll, pitch and yaw rates respectively; and F_x, F_y, and F_z are the components of the sum of external forces in the BRF. The external forces are composed of aerodynamic forces (lift, drag, and lateral force), thrust, and weight.

The aerodynamic forces are the result of the interaction between the airflow and the airframe. These forces can be written as functions of the dynamic pressure $\frac{1}{2}\rho V^2$, wing area S and their respective force coefficients, C_D, C_Y, and C_L, and stability derivatives, as shown in Equations 4, 5, and 6.

$$D = \frac{1}{2}\rho V^2 S\left(C_{D0} + C_{D\alpha}\,\alpha + C_{Dq}\,\frac{qc}{2V} + C_{D\delta_e}\,\delta_e\right) \tag{4}$$
$$Y = \frac{1}{2}\rho V^2 S\left(C_{Y\beta}\,\beta + C_{Yp}\,\frac{pb}{2V} + C_{Yr}\,\frac{rb}{2V} + C_{Y\delta_a}\delta_a + C_{Y\delta_r}\delta_r\right) \tag{5}$$
$$L = \frac{1}{2}\rho V^2 S\left(C_{L0} + C_{L\alpha}\,\alpha + C_{Lq}\,\frac{qc}{2V} + C_{L\delta_e}\,\delta_e\right) \tag{6}$$

Where V is the true airspeed, α is the angle of attack, β is the sideslip angle, δ_a, δ_e, and δ_r are the aileron, elevator, and rudder deflections respectively. The engine thrust is assumed to be produced only in the longitudinal axis of the BRF and to be directly proportional to the thrust lever position. The aircraft weight is rotated from the Inertial Reference Frame (IRF) to the BRF. Thus, the external forces F_x, F_y, and F_z are represented by Equations 7, 8, and 9 respectively.

$$F_x = -D\cos\alpha\cos\beta - Y\cos\alpha\sin\beta + L\sin\alpha + \delta_T\,F_{T_{max}} - m\,g\,\sin\theta \tag{7}$$
$$F_y = -D\sin\beta + Y\cos\beta + m\,g\,\sin\phi\cos\theta \tag{8}$$
$$F_z = -D\sin\alpha\cos\beta - Y\sin\alpha\sin\beta - L\cos\alpha + m\,g\,\cos\phi\cos\theta \tag{9}$$

Where δ_T is the thrust lever position, $F_{T_{max}}$ is the engine's maximum thrust, m is the aircraft mass, and g is the gravity constant. ϕ and θ are the attitude angles for roll and pitch.

2.2 Rotation dynamics

For the angular motion equations, Newton's Second Law for rotational motion is applied. Rearranging the equations and assuming that the aircraft is symmetric in its xz plane, $I_{xy} = I_{xz} = 0$, it is possible to obtain the derivatives of the

roll, pitch and yaw rates $\dot{p}$, $\dot{q}$, and $\dot{r}$, as seen in Equations 10, 11, and 12.

$$\dot{p} = \frac{I_{xz}\,\mathcal{N} + I_{zz}\,\mathcal{L} + I_{xz}(I_{xx} - I_{yy} + I_{zz})\,pq - (I_{xz}^2 - I_{yy}I_{zz} + I_{zz}^2)\,qr}{I_{xx}\,I_{zz} - I_{xz}^2} \tag{10}$$

$$\dot{q} = \frac{\mathcal{M} - (I_{xx} - I_{zz})\,rp - I_{xz}(p^2 - r^2)}{I_{yy}} \tag{11}$$

$$\dot{r} = \frac{I_{xx}\,\mathcal{N} + I_{xz}\,\mathcal{L} + I_{xz}(I_{xx} - I_{yy} + I_{zz})\,qr - (I_{xx}^2 - I_{xx}I_{yy} + I_{xz}^2)\,pq}{I_{xx}\,I_{zz} - I_{xz}^2} \tag{12}$$

The external moments ($\mathcal{L}$, $\mathcal{M}$, and $\mathcal{N}$) are composed of the moments created by the aerodynamic forces and the thrust, because of their point of application in respect to the center of mass. Since the weight is applied in the aircraft center of gravity there is no torque associated with it. Analogous to the aerodynamic forces, the aerodynamic moments are functions of the dynamic pressure, wing area, their respective adimensional force coefficients ($C_{\mathcal{L}}$, $C_{\mathcal{M}}$, and $C_{\mathcal{N}}$), and the wing mean chord c. The torque created by thrust depends on the placement of the engines relative to the aircraft's center of gravity. Since the thrust was considered only in the direction of the aircraft longitudinal axis, it only produces a pitching moment. Equations 13, 14, and 15 depict the rolling, pitching and yawing moments.

$$\mathcal{L} = \frac{1}{2}\,\rho\,V^2\,S\,c\,(C_{\mathcal{L}\beta}\,\beta + C_{\mathcal{L}p}\,\frac{pb}{2V} + C_{\mathcal{L}r}\,\frac{rb}{2V} + C_{\mathcal{L}\delta_a}\delta_a + C_{\mathcal{L}\delta_r}\delta_r) \tag{13}$$

$$\mathcal{M} = \frac{1}{2}\,\rho\,V^2\,S\,c\,(C_{\mathcal{M}0} + C_{\mathcal{M}\alpha}\,\alpha + C_{\mathcal{M}q}\,\frac{qc}{2V} + C_{\mathcal{M}\delta_e}\,\delta_e) + \delta_T\,F_{T_{max}}\,z_T \tag{14}$$

$$\mathcal{N} = \frac{1}{2}\,\rho\,V^2\,S\,c\,(C_{\mathcal{N}\beta}\,\beta + C_{\mathcal{N}p}\,\frac{pb}{2V} + C_{\mathcal{N}r}\,\frac{rb}{2V} + C_{\mathcal{N}\delta a}\delta_a + C_{\mathcal{N}\delta_r}\delta_r) \tag{15}$$

2.3 Rotation kinematics

A relationship between the variation of the Euler's angles for roll ($\dot{\phi}$), pitch ($\dot{\theta}$) and yaw ($\dot{\psi}$), and the rolling, pitching and yawing rates (p, q, and r), can be obtained through a succession of rotations from intermediate planes between the BRF and the IRF. Equations 16 through 18 show the attitude angle variations.

$$\dot{\phi} = p + q\,\sin\phi\tan\theta + r\,\cos\phi\tan\theta \tag{16}$$

$$\dot{\theta} = q\,\cos\phi - r\,\sin\phi \tag{17}$$

$$\dot{\psi} = q\,\sin\phi/\cos\theta + r\,\cos\phi/\cos\theta \tag{18}$$

2.4 Wind model

Wind speed is the speed of the atmosphere in relation to the ground. It affects the aircraft's ground speed, altering its relationship with the true airspeed. Figure 1 illustrates the relationship between ground speed ($\vec{\mathbf{V}}_{\mathbf{G}}$), true airspeed ($\vec{\mathbf{V}}_{\mathbf{A}}$) and wind speed ($\vec{\mathbf{V}}_{\mathbf{W}}$):

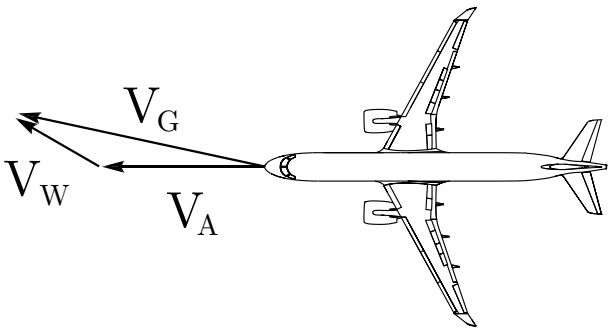

Figure 1: Relationship between ground speed, true airspeed, and wind speed.
Adapted from Embraer (2017).

Because of this relationship, it is possible to define the ground speed as a sum of a true airspeed component and a wind speed component. Breaking the ground speed in speeds in the North, East, and Down directions in the IRF, the ground

speed is expressed by Equations 19 through 21.

$$V_N = V\cos\alpha\cos\beta\cos\theta\cos\psi + V\sin\beta(\sin\phi\sin\theta\cos\psi - \cos\phi\sin\psi) + \\ +V\sin\alpha\cos\beta(\cos\phi\sin\theta\cos\psi + \sin\phi\sin\psi) + V_{WN} \tag{19}$$

$$V_E = V\cos\alpha\cos\beta\cos\theta\sin\psi + V\sin\beta(\sin\phi\sin\theta\sin\psi + \cos\phi\cos\psi) + \\ +V\sin\alpha\cos\beta(\cos\phi\sin\theta\sin\psi - \sin\phi\cos\psi) + V_{WE} \tag{20}$$

$$V_D = -V\cos\alpha\cos\beta\sin\theta + V\sin\beta\sin\phi\cos\theta + V\sin\alpha\cos\beta\cos\phi\cos\theta + V_{WD} \tag{21}$$

Wind speed variations can be considered much slower than the airspeed variations so that they do not affect the ground speed dynamics as much as the airspeed dynamics. Considering the wind speed constant, the dynamics of the true airspeed, angle of attack, and sideslip angle can be written as Equations 22, 23, and 24, respectively.

$$\dot{V} = \dot{u}\cos\alpha\cos\beta + \dot{v}\sin\beta + \dot{w}\sin\alpha\cos\beta \tag{22}$$

$$\dot{\alpha} = \frac{\dot{w}\cos\alpha - \dot{u}\sin\alpha}{V\cos\beta} \tag{23}$$

$$\dot{\beta} = \frac{\dot{v} - \dot{V}\sin\beta}{V\cos\beta} \tag{24}$$

2.5 Atmospheric Model

An atmospheric model presents the mathematical equations to estimate atmospheric variables, such as air temperature, density, and pressure. With the International Standard Atmosphere (ISA) model it is possible to obtain those variables with only the altitude. Figure 2 shows the atmospheric temperature and density varying with the altitude H from sea level up to 71 km.

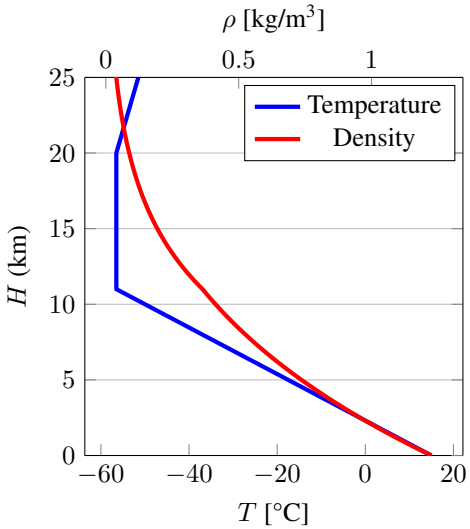

Figure 2: ISA model atmospheric temperature T and and air density ρ at different altitudes.

Since most aircraft have an altitude ceiling limitation, only the first part of the ISA will be considered: from sea level up to 11 km of altitude at a constant temperature gradient. Solving the atmospheric equations in which the temperature is linear from sea-level up to 11 km will result in Equations 25, 26, and 27, for air density, atmospheric temperature, and pressure respectively.

$$\rho = \rho_0\left(1 + \frac{dT}{T_0}H\right)^{\frac{-1}{dT}\left(\frac{g}{R}+dT\right)} \tag{25}$$

$$T = T_0 + dT\,H \tag{26}$$

$$P = \rho\,R\,T \tag{27}$$

Where ρ_0 is the air density at sea-level of 1.225 kg/m^3, T_0 is the temperature at sea-level of 15 °C, and dT is the temperature gradient of -6.5 °C/km.

3. ESTIMATION MODEL

3.1 Direct estimation

A computational procedure was designed to determine angle of attack in Myschik and Sachs (2012) and sideslip angle in Heller *et al.* (2003). The equations used in the process are Equation 28 and Equation 29 respectively.

$$\tilde{\alpha} = \frac{-\left[C_{L0} + \frac{qc}{2V} C_{Lq} + C_{L\delta_e}\,\delta_e\right] \frac{\rho V^2 S}{2m} - a_z}{C_{L\alpha}\,\frac{\rho V^2 S}{2m} + a_x} \tag{28}$$

$$\tilde{\beta} = \frac{1}{C_{Y\beta}} \left[\frac{2m}{\rho V^2 S} a_y - \frac{pb}{2V} C_{Yp} - \frac{rb}{2V} C_{Yr} - C_{Y\delta_r}\,\delta_r\right] \tag{29}$$

Where a_x, a_y, and a_z are the accelerometers readings in the x, y, z directions in the BRF. These equations can be derived from the aerodynamic force equations, making a small angle approximation. These methods for estimating AoA and SSA are still dependent on the true airspeed, which can be approximated by the speed measurement from the GPS velocities, as in Equation 30.

$$\tilde{V} = \sqrt{V_N^2 + V_E^2 + V_D^2} \tag{30}$$

Even though the GPS velocities are derived from the sum of wind and true airspeed, as explained in subsection 2.4, it is possible to make this approximation for wind speeds significantly smaller than the true airspeed. This estimation method has as advantages:

- It is computationally simple: it uses few equations and does not need iteration nor recursion;
- Does not need the complete aircraft model and its aerodynamic coefficients: only lateral force and lift stability coefficients are necessary, geometric constants as wing area, wingspan, mean chord length, and mass.

And as disadvantages:

- The equations are approximations: deviations from the approximation assumptions will cause estimation errors. This method might not be adequate for aircraft flying with a high angle of attack, or small UAV flying in intense wind fields;
- There is no way to estimate the wind speed: since the true airspeed is an approximation of the ground speed, an attempt to estimate the wind speed will result in a zero wind speed;

3.2 Extended Kalman filter

The Kalman filter is an optimal recursive estimator Aguirre (2015). It is a linear system state estimator that uses measurements to reduce the estimation error. The Extended Kalman filter (EKF) is the non-linear version of the Kalman filter, which is a near-optimal estimator due to the non-linearities of the system. The EKF algorithm can be summarized in two steps: prediction and update.

For the prediction step, an estimate of the states is made based on past states and the dynamic model and current inputs. The more representative of the real system a model is, the more accurate will be the prediction. Equation 31 is the state prediction equation and Equation 32 is the covariance of the prediction equation.

$$\mathbf{x}_k^- = f(\mathbf{x}_{k-1}^-, \mathbf{u}_k) \tag{31}$$

$$\mathbf{P}_k^- = \mathbf{F}_k\,\mathbf{P}_{k-1}^-\,\mathbf{F}_k^\top + \mathbf{Q} \tag{32}$$

Where f is the state estimation function, $\mathbf{x}_k^-$ is the current state vector, $\mathbf{x}_{k-1}^-$ is the past state vector, $\mathbf{u}_k$ is the inputs vector, $\mathbf{P}$ is the state covariance matrix, $\mathbf{F}$ is the Jacobian matrix of function $f(\mathbf{x}_{k-1}^-, \mathbf{u}_{k-1})$, and $\mathbf{Q}$ is the process covariance matrix, which is a diagonal matrix with the covariance ${\sigma^2}_x$ of all states.

For discrete time the state estimation is done numerically using the Newton-Raphson's integration method, as described in Equation 33:

$$\mathbf{x}_k^- = \mathbf{x}_{k-1}^- + \dot{f}(\mathbf{x}_{k-1}^-, \mathbf{u}_k)\,\Delta t \tag{33}$$

For the prediction model of this work, the chosen states and inputs can be seen in Equations 34 and 35 respectively.

$$\mathbf{x} = \begin{bmatrix} V & \alpha & \beta & u & v & w & p & q & r & \phi & \theta & \psi & H \end{bmatrix}^\top \tag{34}$$

$$\mathbf{u} = \begin{bmatrix} \delta_a & \delta_e & \delta_r & \delta_\pi \end{bmatrix}^\top \tag{35}$$

The process covariance matrix is defined by Equation 36.

$$\mathbf{Q} = \text{diag}\begin{pmatrix} \sigma_V^2 & \sigma_\alpha^2 & \sigma_\beta^2 & \sigma_u^2 & \sigma_v^2 & \sigma_w^2 & \sigma_p^2 & \sigma_q^2 & \sigma_r^2 & \sigma_\phi^2 & \sigma_\theta^2 & \sigma_\psi^2 & \sigma_H^2 \end{pmatrix} \tag{36}$$

For the update step, the states and covariance matrix will be calculated with a correction based on the measurement of the system. The process for updating the states based on this correction is shown in Equations 37, 38, and 39.

$$\mathbf{K}_k = \mathbf{P}_k^- \, \mathbf{H}_k^\top (\mathbf{H}_k \, \mathbf{P}_k^- \, \mathbf{H}_k^\top + \mathbf{R}_k) \tag{37}$$

$$\mathbf{x}_k^+ = \mathbf{x}_k^- + \mathbf{K}_k \left(\mathbf{z}_k - h(\mathbf{x}_k^-, \mathbf{u}_k)\right) \tag{38}$$

$$\mathbf{P}_k^+ = (\mathbf{I} - \mathbf{K}_k \, \mathbf{H}_k) \, \mathbf{P}_k^- \tag{39}$$

Where $\mathbf{K}_k$ is the Kalman gain, $\mathbf{z}_k$ is a vector of measurements taken, the function $\mathbf{h}(\mathbf{x}_k^-, \mathbf{u}_k))$ is the observation function which relates the sensors inputs and the system states and inputs, $\mathbf{H}$ is the Jacobian matrix of the observation function $h(x_k)$, and $\mathbf{R}$ is the measurement covariance matrix, which is a diagonal matrix with the covariance $\sigma^2{}_y$ of all measurements.

The Kalman gain is a correction factor that takes into consideration the predicted covariance matrix and the covariance of the measurements, which are based on the precision of the sensors used. This gain is an indication of what is more precise: estimate or measurement, based on their covariance. The Kalman gain will "correct" the estimate and reduce its covariance. For the next iterations, if the system is properly initialized and uses a good dynamic model, the estimate covariance will be lower and lower, until convergence is reached. To reach convergence of the estimates, the process is repeated looping the estimates for the next discrete-time measurements.

The measurement model is built considering the availability of sensors in the aircraft. Only inertial sensors will be used in this work. Those sensors will provide the necessary data to increase the precision of the filter. Equation 40 shows the variables measured by the available sensors.

$$\mathbf{y} = \begin{bmatrix} V_N & V_E & V_D & a_x & a_y & a_z & p & q & r & \phi & \theta & \psi & H \end{bmatrix}^\top \tag{40}$$

V_N, V_E, and V_D are velocities measurements in the IRF made by the GPS unit. a_x, a_y, and a_z are accelerations in the longitudinal, lateral and vertical axis of the aircraft, measured by the IMU accelerometers. Estimations of roll, pitch, and yaw rates: p, q, and r, respectively, and attitude angles of roll ϕ, pitch θ, and yaw ψ respectively, are made by the IMU gyroscopes. H is given by the GPS unit, which measures the geometric altitude measurement and not the pressure altitude.

The measurement covariance matrix is defined by Equation 41.

$$\mathbf{R} = \text{diag}\begin{pmatrix} \sigma_{V_N}^2 & \sigma_{V_E}^2 & \sigma_{V_D}^2 & \sigma_{a_x}^2 & \sigma_{a_y}^2 & \sigma_{a_z}^2 & \sigma_p^2 & \sigma_q^2 & \sigma_r^2 & \sigma_\phi^2 & \sigma_\theta^2 & \sigma_\psi^2 & \sigma_H^2 \end{pmatrix} \tag{41}$$

4. RESULTS

Both models, the Direct Estimation (DE) and the Extended Kalman Filter (EKF) were used to estimate flight data of a flight test of the C2 Unmanned Aerial Vehicle. Table 1 shows some of the geometry parameters of the aircraft and Figure 3 depicts a transparent picture of the UAV.

Table 1: Aircraft constants

S [m^2]	b [m]	c [m]	m [kg]	$F_{T_{max}}$ [N]
2.223	5.000	0.454	60.00	300.0

The flight data used for the estimation was a fraction of the flight test, where two successive doublets were applied on the elevators, while other control commands are kept constant. The elevator maneuver is shown in Figure 4.

To employ the estimation methods, the aircraft mathematical model used was the same used in section 3. The aircraft parameters, such as inertia matrix, stability derivatives, and others, can be found in Sarmento (2020). The covariance matrices for the Extended Kalman Filter were defined as in Equation 42 and Equation 43 using the constants in Table 2.

$$\begin{aligned} \mathbf{Q} = \text{diag}\Big(&\sigma_V^2 \quad \sigma_\alpha^2 \quad \sigma_\beta^2 \quad 0.1\sigma_{\mathbf{V_B}}^2 \quad 0.1\sigma_{\mathbf{V_B}}^2 \quad 0.1\sigma_{\mathbf{V_B}}^2 \quad \dots \\ &0.1\sigma_\omega^2 \quad 0.1\sigma_\omega^2 \quad 0.1\sigma_\omega^2 \quad 0.1\sigma_\Theta^2 \quad 0.1\sigma_\Theta^2 \quad 0.1\sigma_\Theta^2 \quad 0.1\sigma_H^2\Big) \end{aligned} \tag{42}$$

$$\mathbf{R} = \text{diag}\begin{pmatrix} \sigma_{V_{GPS}}^2 & \sigma_{V_{GPS}}^2 & \sigma_{V_{GPS}}^2 & \sigma_{\mathbf{a}}^2 & \sigma_{\mathbf{a}}^2 & \sigma_{\mathbf{a}}^2 & \sigma_\omega^2 & \sigma_\omega^2 & \sigma_\omega^2 & \sigma_\Theta^2 & \sigma_\Theta^2 & \sigma_\Theta^2 & \sigma_{P_{GPS}}^2 \end{pmatrix} \tag{43}$$

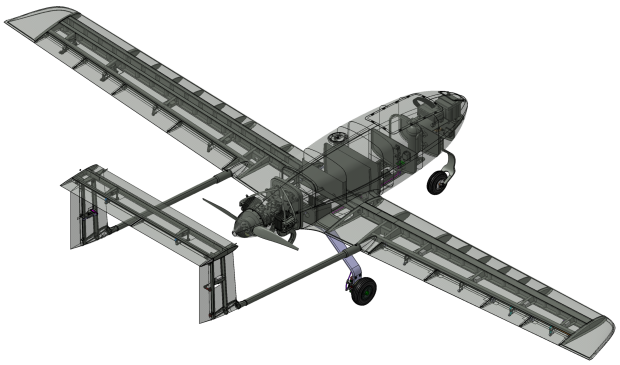

Figure 3: C2 Unmanned Aerial Vehicle.
Adapted from Sarmento (2020).

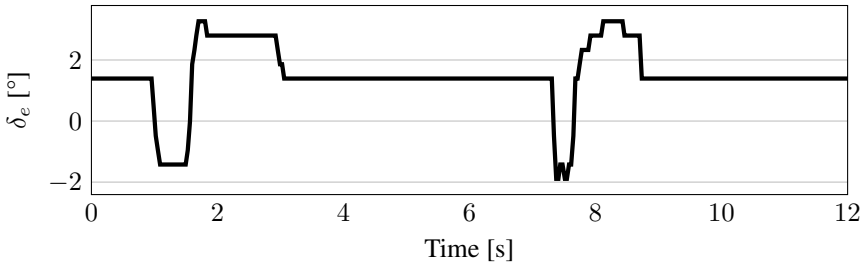

Figure 4: Flight test elevator doublet.

Table 2: Covariances for each instrument

Instrument	**Symbol**	**Variance**
GPS Unit (velocity)	$\sigma^2_{V_{GPS}}$	0.100 m^2/s^2
GPS Unit (position)	$\sigma^2_{P_{GPS}}$	1.000 m^2
Accelerometer	$\sigma^2_{\mathbf{a}}$	0.050 m^2/s^4
Gyrometer	σ^2_{ω}	0.001 rad^2/s^2
Gyroscope	σ^2_{Θ}	0.010 rad^2
Probe (TAS)	σ^2_{V}	0.100 m^2/s^2
Probe (AoA)	σ^2_{α}	0.001 rad^2
Probe (SSA)	σ^2_{β}	0.001 rad^2

These values are conservative values, obtained through calculating the covariance of the measurements of the flight test. Estimation results for both methods are displayed in Figure 5.

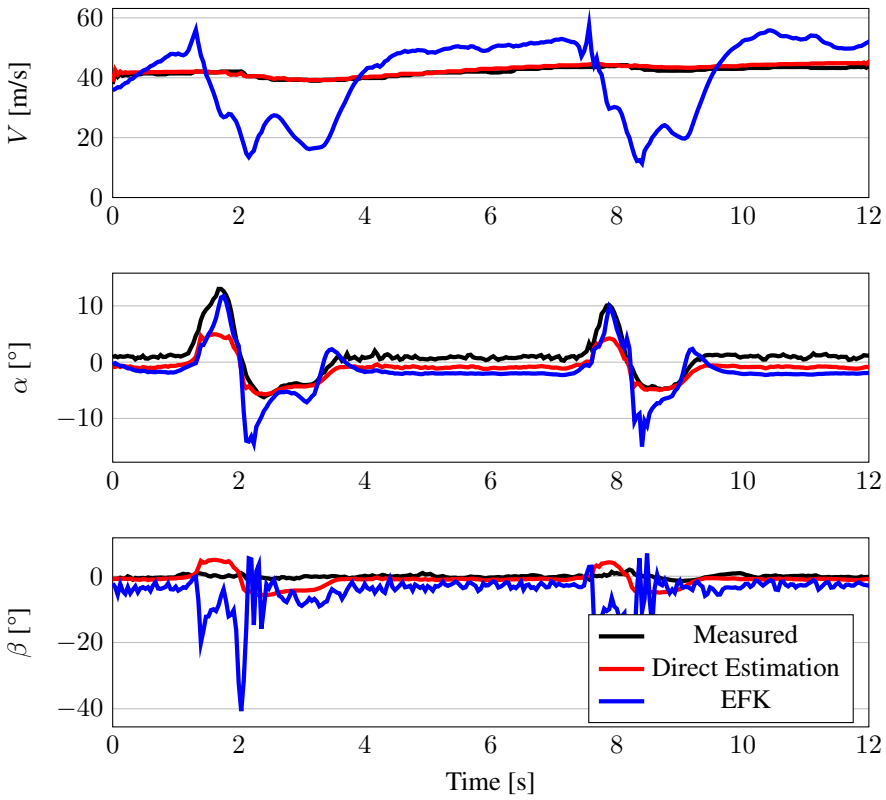

Figure 5: Estimation of True Airspeed, Angle of Attack and Sideslip Angle using an untuned model

The estimators cannot produce a reliable result if the mathematical model is not well defined. The Extended Kalman filter still reaches convergency, due to the good definition of the process and measurement covariance matrices. Taking the measured values as the expected values, the NRMSE for this estimation is seen on Table 3.

Table 3: RMS Error for the untuned estimation.

	DE	**EKF**
e_V [%]	1.90	30.27
e_α [%]	302.64	417.97
e_β [%]	2195.89	7194.62

To increase the estimation model's performance, an attempt to tune the aircraft mathematical model was made. The mathematical model was tuned manually, adjusting the aerodynamic coefficients so that the estimators could somewhat converge to the expected values of true airspeed, angle of attack, and sideslip angle. The geometric constants of the aircraft have not been changed, as they were expected to be correct. After the aerodynamic forces coefficients were updated, the aerodynamic moment coefficients were updated, using the estimations of roll, pitch, and yaw rates. These variables are dependent on the rolling, pitching, and yawning moments respectively, so they were tuned until a good result was reached in the EKF estimation. Figure 6 depicts the estimations of V, α, and β, after updating the aerodynamic coefficients of the aircraft model.

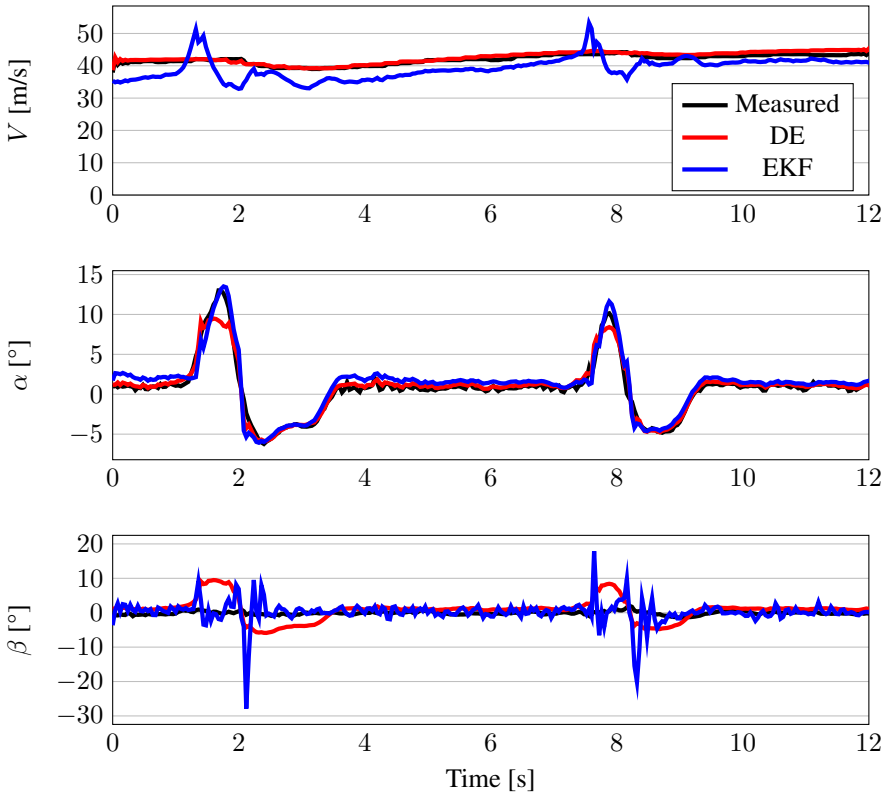

Figure 6: Estimation of True Airspeed, Angle of Attack and Sideslip Angle using a tuned model.

This empirical tuning method is far from being optimal, and producing a well-tuned model is not an objective of this work. Still, it was done so that the estimation methods could be implemented and produce data with a better level of precision. For future work, it is recommended that a proper parameter identification method is used to tune the mathematical model. Table 4 shows the estimation errors for the tuned model.

Table 4: RMS Error for the tuned estimation.

	DE	**EFK**
e_V [%]	1.90	10.03
e_α [%]	138.37	128.50
e_β [%]	3077.00	3114.25

5. CONCLUSION

The Direct Estimation and the Extended Kalman Filter methods were used to estimate air data from the flight test data in the early stages of a model identification campaign. In these stages, the Direct Estimation method produced lesser estimation errors, which was expected, as it is not as dependant on the model as the Extended Kalman Filter method. It is noted that the control surface deflection seen in the flight test data was small, which, coincidentally, took the method limitation into account.

As the aircraft model identification campaign progresses, it is expected that the Extended Kalman Filter produces lesser estimation errors, as seen in section 4. Although the Direct Estimation method continues to produce accurate results compared to the EKF method with a fully identified model, the limitation of being unable to estimate the wind speed is a downside. It is recommended that when the model is accurate enough, the EKF method is used in favor of the DE method, because of the importance of wind speed estimation in real applications.

Although the methods have the means to estimate the sideslip angle, there was no estimation of it based on the excitation of the lateral dynamics in the simulations or flight test data. Upon further inspection of the provided aircraft model, its lateral dynamics model was intrinsically unstable, rendering the estimations impracticable.

6. REFERENCES

Aguirre, L., 2015. *Introdućão à Identificaćão de Sistemas*. ISBN 978-85-423-0079-6. doi:10.13140/RG.2.1.1616.7925.
Edward A. Haering, J., 1995. “Airdata measurement and calibration”. Technical report, NASA.

Embraer, 2017. *E-Jets E2 Airport Plannning Manual*. URL https://www.flyembraer.com/irj/go/km/docs/download_center/Anonymous/Ergonomia/Home%20Page/Documents/APM_E-JetsE2.PDF.

Heller, M., Myschik, S., Holzapfel, F. and Sachs, G., 2003. "Low-cost approach based on navigation data for determining angles of attack and sideslip for small air-craft."

Moes, T.R. and Whitmore, S.A., 1990. "A preliminary look at techniques to obtain airdata from flight at high angles of attack". Technical report, NASA.

Myschik, S. and Sachs, G., 2012. "Flight testing an integrated wind/airdata- and navigation system for general aviation aircraft". doi:10.2514/6.2007-6796. URL https://arc.aiaa.org/doi/abs/10.2514/6.2007-6796.

Sarmento, A.G.P., 2020. *Instrumentaćão e controle de um VANT agrícola*. Master's thesis, Instituto Tecnológico de Aeronáutica.

7. RESPONSIBILITY NOTICE

The authors are solely responsible for the printed material included in this paper.